Geomechanics and Engineering, *Vol. 29, No. 5 (2022) 583-598*
https://doi.org/10.12989/gae.2022.29.5.583

Field experimental study for layered compactness of subgrade based on dimensional analysis

Dandan Han[1,2], Zhijun Zhou*[2], Jiangtao Lei[3], Minguo Lin[1] and Haochen Zhan[2]

[1]*Key Laboratory of Ministry of Education for Geomechanics and Embankment Engineering, Hohai University, Nanjing, Jiangsu, 210098, The People's Republic of China*
[2]*School of Highway, Chang'an University, Xi'an, Shaanxi, 710064, The People's Republic of China*
[3]*Division of Geotechnical Engineering and Geosciences, Department of Civil and Environmental Engineering, Polytechnic University of Catalonia (UPC), Spain*

(Received October 20, 2021, Revised March 20, 2022, Accepted March 25, 2022)

Abstract. The Compaction effect is important for evaluating the subgrade construction. However, there is little research exploring the compaction quality of deep soil using hydraulic compaction. According to reinforcement effect analysis, dimensional analysis is adopted in this work to analyze subgrade compactness within the effective reinforcement depth, and a prediction model is obtained. A hydraulic compactor is then employed to carry out an in-situ reinforcement test on gravel soil subgrade, and the subgrade parameters before and after reinforcement are analyzed. Results show that a reinforcement difference exists inside the subgrade, and the effective reinforcement depth is defined as increasing compactness to 90% in the depth direction. Layered compactness within the effective reinforcement depth is expressed by parameters including the drop distance of the rammer, peak acceleration, tamping times, subgrade settlement, and properties of rammer and filler. Finally, a field test is conducted to verify the results.

Keywords: compactness; dimensional analysis; gravel soil subgrade; hydraulic compaction; road engineering

1. Introduction

Dynamic compaction is one of the most effective methods for subgrade reinforcement that can effectively improve soil strength and compactness (Hu *et al.* 2018, Ghanbari *et al.* 2014). However, it is difficult to operate the dynamic compaction machinery used for small-size construction projects, such as abutment, which can create safety hazards (Huang *et al.* 2014, Zhang *et al.* 2013, Carter *et al.* 2015, Javier *et al.* 2017, Ma *et al.* 2014). In contrast, hydraulic compaction is flexible, efficient, and most importantly, can be applied to special subgrade sections like the backside of abutments (Adam *et al.* 2011, Allouzi *et al.* 2019, Dobrzycki *et al.* 2019, Wu and Sang 2012).

Highway construction has developed rapidly in China in recent years. The total length and maintenance mileage of highways is increasing annually, and the maintenance expenditure is huge, mainly because the subgrade is relatively complex (Fig. 1). When the compactness of the subgrade fails to meet the requirements, longitudinal cracks or pavement cross-sections will occur (Wang 2011, Barman *et al.* 2016, Viyanant *et al.* 2004, Xu *et al.* 2018, Kodikara *et al.* 2018). Therefore, it is of great significance to monitor compactness during the subgrade construction process. Previous studies have mainly focused on the evaluation of the compactness and settlement of the subgrade (Zhang *et al.* 2013, Erem'yants and Uraimov 2009, Gu and Xiong 2008, Meehan *et al.* 2012, Min *et al.* 2020, Wersall *et al.* 2018, Tehrani *et al.* 2014, Nie 2011, Meehan *et al.* 2017, Cai *et al.* 2017). This research is largely centered on the deformation characteristics of the subgrade surface, ignoring the deep soil compactness of the subgrade (Senseney and Mooney 2010). While some scholars have considered deep soil compactness, their evaluation methods are destructive and intermittent in the detection process, which is also difficult to control in practical engineering (White *et al* 2005, Herrera *et al* 2018, Rinehart *et al* 2012, Pistrol and Adam 2018, Ling 2018).

At present, only a few works examine the compaction quality of deep soil using hydraulic compaction. Based on the collision theory in the elastic half space, Xu *et al.* (2020) proposed a calculation method to explore the relationship between the compactness of deep soil of subgrade and the peak acceleration of rammer. Zhang *et al.* (2021) established the basic model of hydraulic compaction and the relationship between layered compactness before and after reinforcement using layered compaction theory. However, these works ignored dimensional unification and the interaction of tamping points (Butterfield 2001, Zhou *et al.* 2019, Dimitrakopoulos *et al.* 2010). Further, the above works were carried out in a road test tank (using rigid constraints to limit the diffusion of tamping energy), meaning that the measured compactness of the model test would be larger than that of an actual project under the same conditions. The hydraulic compactor, construction parameters and subgrade filler can also influence the reinforcement effect in practical engineering (Wang and

*Corresponding author, Professor
E-mail: zhouzhijun@chd.edu.cn

ISSN: 2005-307X (Print), 2092-6219 (Online)

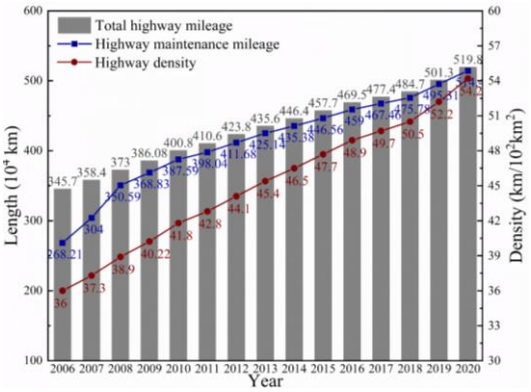

(a) Summary of highway construction and maintenance

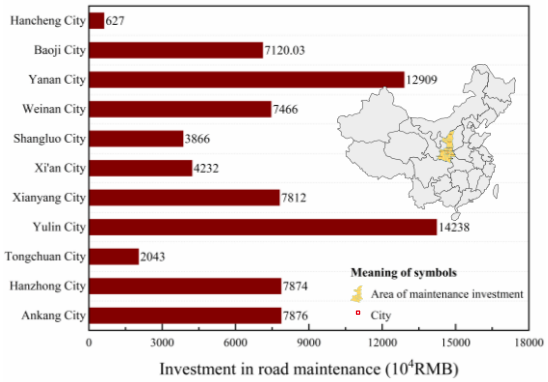

(b) Investment distribution of highway maintenance in Shaanxi Province in 2020

Fig. 1 China's highway development from 2011 to 2020 (Source: the Ministry of Transport of the People's Republic of China)

Liao 2012, Cai *et al.* 2013). Hence, in this study, the relationship between the compactness of deep soil and influencing parameters of reinforcement effect is obtained using dimensional analysis. The settlement and compactness of the subgrade before and after reinforcement are analyzed by in-situ reinforcement test to obtain the effective reinforcement depth (H). A calculation method to determine the layered compactness of subgrade within the effective reinforcement depth is then proposed. Finally, this calculation method is verified considering different soils, indicating that the test results are generally applicable.

2. Dimensional analysis

2.1 Basic principles of dimensional analysis

Dimensional analysis was proposed in the early 20th century for establishing mathematical models in the field of physics. It is an effective means to study scientific laws and solve engineering problems. On the basis of experience and experiments, the dimensions of physical variables related to problems are expressed by basic dimensions, and dimensionless quantities containing variables are obtained by the principle of dimensional homogeneity. Dimensional analysis has been applied in numerous fields, including geotechnical expansion and structural collision (Buzzi *et al.* 2011, Wu *et al.* 2019, Dimitrakopoulos *et al.* 2009b).

The Π theorem is the theoretical core of dimensional analysis. If a physical problem has n variables (ω_1, ω_2, ⋯, ω_n), the functional relationship of dependent variable ω is expressed as

$$\omega = \xi(\omega_1, \omega_2, \cdots \omega_k, \omega_{k+1}, \cdots \omega_n) = 0 \tag{1}$$

Among them, there are k basic quantities. If they are ranked first among the independent variables, then ω_1, ω_2, ⋯, ω_k are the basic quantities, and their dimensions are ψ_1, ψ_2, ⋯, ψ_k, respectively. The other (n-k) independent variables are derived quantities, and their dimensions can be expressed as the dimensional power equation of the basic quantities

$$[\omega_m] = \psi_1^{\sigma_m} \psi_2^{\tau_m} \cdots \psi_k^{\delta_m}, \quad k < m < n \tag{2}$$

The dimension of dependent variable ω is

$$[\omega] = \psi_1^{\sigma} \psi_2^{\tau} \cdots \psi_k^{\delta} \tag{3}$$

Where σ_m, τ_m, ⋯, δ_m; σ, τ,⋯, δ are the corresponding power values.

The basic quantity ω_1, ω_2, ⋯, ω_k is employed to measure the above functional relationship

$$\omega / \left(\omega_1^{\sigma} \omega_2^{\tau} \cdots \omega_k^{\delta}\right) = \xi \begin{pmatrix} 1,1,\cdots 1; \omega_{k+1} / \left(\omega_1^{\sigma_{k+1}} \omega_2^{\tau_{k+1}} \cdots \omega_k^{\delta_{k+1}}\right); \\ \omega_{k+2} / \left(\omega_1^{\sigma_{k+2}} \omega_2^{\tau_{k+2}} \cdots \omega_k^{\delta_{k+2}}\right); \cdots \omega_n / \left(\omega_1^{\sigma_n} \omega_2^{\tau_n} \cdots \omega_k^{\delta_n}\right) \end{pmatrix} \tag{4}$$

The left end of the above formula is a dimensionless dependent variable, which is recorded as Π. The last (n-k) dimensionless dependent variables at the left and are recorded as Π_1, Π_2, ⋯, Π_{n-k}; then, the dependent variable Π is $\Pi = g(\Pi_1, \Pi_2, \cdots, \Pi_{n-k})$, and the equivalent equation of Eq. (1) is

$$g(\Pi_1, \Pi_2, \cdots, \Pi_{n-k}) = 0 \tag{5}$$

2.2 Analysis on Influencing factors of subgrade compactness

Hydraulic compaction is a method that converts the gravitational potential energy into kinetic energy to compact subgrade. During hydraulic compaction, soil particles will produce mutual displacement under the external force. The soil under the rammer moves to the depth, and the surrounding soil remains stationary, or the displacement is small enough to form a shear surface. The gravel enhances the shear strength of the filler during this process (Sabbar *et al.* 2018). The reinforcement mechanism is shown in Fig. 2.

The existing research shows that diffusion/ absorption of tamping energy is affected by the rammer and subgrade filler. Therefore, the compactness evaluation of subgrade is a complex engineering problem (Yao and Zhang 2016, Feng

Table 1 Physical quantities involved under compaction

	Physical quantity	Dimension
Dependent variable	Settlement of subgrade (u)	$L^1M^0T^0$
	Compactness of Subgrade (K)	-
Independent variable	Peak acceleration of rammer (a)	$L^1M^0T^{-2}$
	Weight of rammer (Q)	$L^1M^1T^{-2}$
	Drop distance of rammer (h)	$L^1M^0T^0$
	Tamping times (N)	-
	Bottom area of rammer (A)	$L^2M^0T^0$
	Soil-rock ratio (P)	-
	Density of filler (ρ)	$L^{-3}M^1T^0$
	Cohesion of filler (c)	$L^{-1}M^1T^{-2}$

*Note: "-" indicates dimensionless coefficient

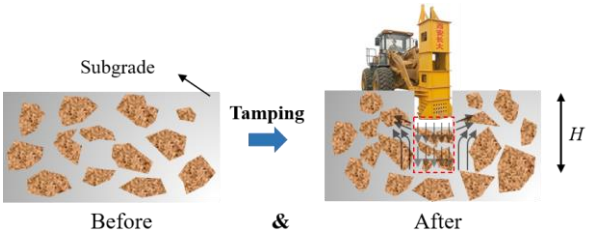

Fig. 2 Schematic diagram of reinforcement mechanism

et al. 2012, Bai *et al.* 2020, Mei *et al.* 2016). As geotechnical engineering problems are too complex to be expressed by simple mathematical equations, dimensional analysis is used to simplify the factors affecting the reinforcement effect (Butterfield 2001). The parameters involved in reinforcement include peak acceleration, the weight and bottom area of the rammer, drop distance, tamping times, subgrade settlement, compactness, soil-rock ratio, density and filler cohesion. The dimensions of the above parameters are shown in Table 1 (Anderegg and Kaufmann 1868, Xing *et al.* 2019, Hua *et al.* 2018, Xia and Li 2015, Xing, Liu and Luo 2019, Xu, Li and Zhang 2015, Xu, Song and Cao 2009).

As described by Zhang *et al.* (2021) and Xu *et al.* (2020), the tamping energy reinforces the subgrade within the effective reinforcement depth (Nazhat and Airey 2015). There is also a dynamic displacement response relationship between the rammer and subgrade during reinforcement (Parvizi 2009, Mayne *et al.* 1984, Gruzin *et al.* 2018, Thilakasiri *et al.* 1996, Arias-Lara and De-la-Colina 2018). That is, the peak acceleration of rammer and the settlement of subgrade reflect the subgrade compaction state, which provides a theoretical basis to establish a dimensionless model.

2.3 Construction of dimensionless model

2.3.1 Dimensionless model of surface compactness

According to the previous analysis, different parameters can be used to quantify the compactness of subgrade, which is mainly affected by the hydraulic compaction, construction parameters and subgrade. Therefore, the compactness after reinforcement can be expressed as

$$K = f\left(u,a,Q,h,N,A,P,\rho,c\right) \tag{6}$$

Where K is the compactness of subgrade surface, N and P are dimensionless coefficients, which are not discussed in the dimensional analysis. Therefore, Eq. (6) can be simplified to Eq. (7)

$$K = f\left(u,a,Q,h,A,\rho,c\right) \tag{7}$$

The physical relationship between the parameters is determined according to the properties of each physical quantity and correlation. At the same time, the dimension of Eq. (7) is normalized according to the principle of dimensional unification, and u, a, Q are selected as independent dimensions to represent other physical quantities

$$K = f\left(h/u, A/u^2, u^3a\rho/Q, u^2c/Q\right) \tag{8}$$

Where $\pi_1=h/u$, $\pi_2=A/u^2$, $\pi_3=u^3a\rho/Q$, $\pi_4=u^2c/Q$. Since the multiplication of dimensionless parameters and power are dimensionless quantities (Buzzi 2010, Buzzi *et al.* 2011), $(\pi_1\cdot\pi_2\cdot\pi_3\cdot\pi_4)^{1/3} = au^2h\cdot\rho cA/Q^2$ is a dimensionless parameter, so that $K\sim au^2h\cdot\rho cA/Q^2$ has a functional relationship. Finally, the compactness after reinforcement can be expressed as

$$\left.\begin{aligned}\ln K &= \alpha_1' + \beta_1 \ln\left[\left(au^2h\right)\cdot\rho cA/Q^2\right]\\ &= \ln\left[\alpha_1\cdot\left(au^2h\cdot\rho cA/Q^2\right)^{\beta_1}\right]\end{aligned}\right\} \Rightarrow K = \alpha_1\cdot\left[\left(au^2h\right)\cdot\rho cA/Q^2\right]^{\beta_1} \tag{9}$$

For the same test, ρ, c, A and Q are the same; that is, $\rho cA/Q^2$ are constants. α_1 is the dimensionless coefficient in the above mathematical expression, which is mainly related to N and P. According to the relationship curve between on-site compactness and tamping times, the subgrade compactness and tamping times have a power function ($K\sim N^\gamma$), and the compactness increases with the increase of tamping times. This rising trend gradually slows down and finally tends to be stable. α_1 is obtained as

$$\alpha_1 = \varphi\left(N,\mathrm{P}\right) \Rightarrow \alpha_1 = \lambda_1 N^{\gamma_1} + \mu_1 \tag{10}$$

Where λ_1, γ_1 and μ_1 are dimensionless coefficients.

To summarize, the calculation equation of the surface compactness of the subgrade is

$$K=\left(\lambda_1 N^{\gamma_1}+\mu_1\right)\cdot\left(au^2h\cdot\rho cA/Q^2\right)^{\beta_1} \tag{11}$$

2.3.2 Dimensionless model of effective reinforcement depth

The reinforcement of the hydraulic compaction is accompanied by energy loss. The improvement in compactness gradually slows down with increasing depth of subgrade (Yan *et al.* 2011). The depth where compactness increased from 86.5% to 90% is taken as the effective reinforcement depth in this work.

While scholars have studied the calculation of the effective reinforcement depth of dynamic compaction (Li 2018), the dimension is ignored, making it impossible to perform transcendental function calculations. Therefore, in this study, the effective reinforcement depth is obtained based on dimensional analysis.

$$H=\theta(Q,h,N,A,P,\rho,c)\Rightarrow H=\theta(Q,h,A,\rho,c) \tag{12}$$

Taking Q, h and ρ as independent dimension, the following can be obtained

$$H/h=\theta\left(A/h^2,h^2c/Q\right) \tag{13}$$

$\pi_1^{1/2}\cdot\pi_2=hcA^{1/2}/Q$ is the dimensionless physical quantity, in which $\pi_2=A/h^2$ and $\pi_2=h^2c/Q$. Therefore, the compactness of subgrade after reinforcement can be expressed as

$$\left.\begin{aligned}H/h&=\alpha_2\cdot\left(hcA^{1/2}/Q\right)^{\beta_2}\\ \alpha_2&=\lambda_2N^{\gamma_2}\end{aligned}\right\}\Rightarrow H=\left(\lambda_2N^{\gamma_2}\right)\left(cA^{1/2}/Q\right)^{\beta_2}\cdot h^{\beta_2+1} \tag{14}$$

2.3.3 Dimensionless model of layered settlement

Previous research shows that the layered settlement of subgrade is related to u, H, h, N and z (Zhang *et al.* 2021). Combined with the influencing parameters of the reinforcement effect, the layered settlement after reinforcement is obtained as

$$u_i=\varphi(u,H,h,N,z)\Rightarrow u_i=\varphi(u,H,h,z) \tag{15}$$

Where u_i is the layered settlement of subgrade.

h is selected as the basic physical quantity to obtain

$$u_i/h=\varphi(u/h,H/h,z/h) \tag{16}$$

Where $\pi_1=u/h$, $\pi_2=H/h$, $\pi_3=z/h$, $(\pi_1\cdot\pi_2\cdot\pi_3^{-1})=uH/hz$ is a dimensionless physical quantity. Therefore, $u_i\sim uH/hz$ is considered to exhibit a functional relationship, and the mathematical model of layered settlement is

$$u_i=\alpha_3\cdot(uH/z)^{\beta_3}h^{1-\beta_3} \tag{17}$$

2.3.4 Dimensionless model of layered compactness

According to relevant literature (Xu *et al.* 2020, Zhang *et al.* 2021), the layered compactness after reinforcement is mainly related to tamping times, the drop distance of the rammer and the subgrade depth, and has a dynamic response relationship with subgrade settlement (including the surface and interior of the subgrade) and the peak acceleration of rammer. At the same time, N and P are not discussed in terms of dimensions and dimensionless coefficients. Therefore, the simplified layered compactness can be expressed as

$$K_i=f\left(u,a,Q,h,N,A,P,\rho,c,u_i\right)\Rightarrow K_i=f\left(u,a,Q,h,A,\rho,c,u_i\right) \tag{18}$$

Where K_i is the layered compactness of the subgrade.

u, a, and Q are taken as the basic physical quantities and can be obtained

$$K_i=f\left(h/u,A/u^2,u^3a\rho/Q,u^2c/Q,u_i/u\right) \tag{19}$$

Where $\pi_1=h/u$, $\pi_2=A/u^2$, $\pi_3=u^3a\rho/Q$, $\pi_4=u^2c/Q$, $\pi_5=u_i/u$; then, $(\pi_1\cdot\pi_2\cdot\pi_3\cdot\pi_4\cdot\pi_5^2)=a^2u_ih\cdot\rho cA/Q^2$. As mentioned above, the layered compactness after reinforcement can be expressed as

$$K_i=\alpha_4\cdot\left[\rho cA/Q^2\cdot\left(au_i^2h\right)\right]^{\beta_4} \tag{20}$$

It can be seen from the above analysis that $\rho cA/Q^2$ is a constant and $\alpha_4=\lambda_4N^{\gamma4}+\mu_4$. According to the principle of dimensional unity, the following can be obtained

$$K_i=\left(\lambda_4N^{\gamma_4}+\mu_4\right)\cdot\left(au_i^2h\cdot\rho cA/Q^2\right)^{\beta_4} \tag{21}$$

3. Test method

3.1 Test site

We conducted a field test on the gravel soil subgrade behind an abutment on Taibai-Fengxian Expressway in Baoji City, Shaanxi Province (Fig. 3). Screen test, compaction, large-scale direct shear, and large-scale consolidation tests were carried out to determine the physical and mechanical properties of the on-site filler (Fig. 4). The corresponding performance index values are provided in Table 2.

A screening test of the on-site filler was first carried out to determine the particle size distribution of the soil sample. The compaction test was conducted according to the on-site grading and batching. The maximum particle size on site exceeds 40 mm. According to the specification (JTG E40-2007), when the maximum particle size exceeds 40 mm and the mass content of the excess part is 5% ~ 30%, the particles exceeding 40 mm must be removed and their percentage obtained. Thus, we conducted compaction tests on the particles less than 40 mm in size. The maximum dry density and optimal moisture content obtained from the test were then corrected, respectively. Three groups of parallel samples were employed, and the relationship curve between the moisture content and dry density of the soil samples under moisture content of 2%, 4.5%, 6%, 8% and 10% were determined. Finally, the optimal moisture content and maximum dry density of samples were obtained.

We used a similar grading method to prepare samples with optimal moisture content. Three groups of samples were taken to obtain the shear stress-shear displacement curve under the

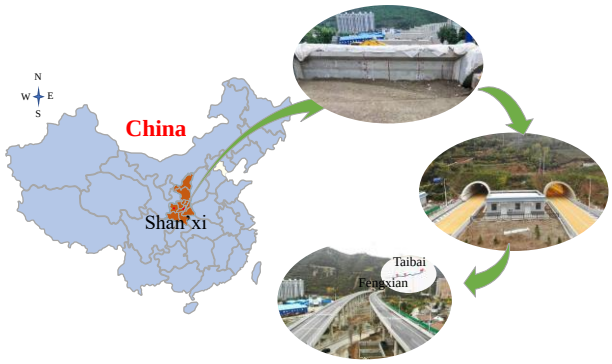

Fig. 3 Geographical location of the study area

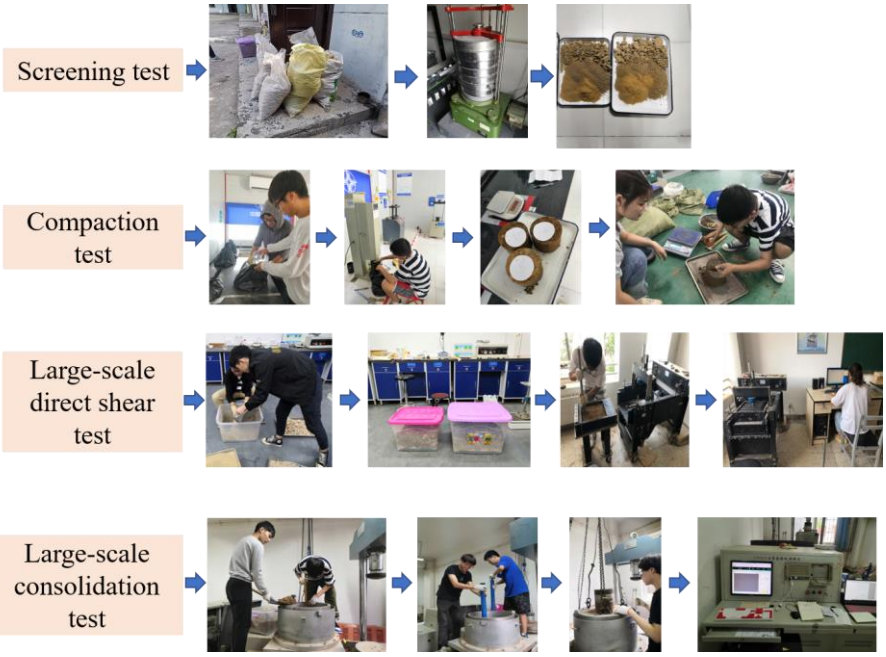

Fig. 4 Flow chart of indoor test

Table 2 Physical and mechanical properties of gravel soil

Maximum dry density /g·cm^{-3}	Optimum moisture content /%	Cohesion /Pa	Internal friction angle /°	Compressibility factor /Mpa^{-1}	Compression modulus /Mpa	Compression index
2.38	3.34	25230	38.36	0.16	7.91	0.053

stress conditions of 100, 200, 400 and 600kpa, respectively, and the normal stress-shear strength lines of the gravel soil were fitted. Finally, the average cohesion and friction angle of sandy gravel soil were obtained as 25.23 kpa and 38.36°, respectively.

A similar grading method was also adopted for the on-site super particle size. A consolidation test was carried out after batching with optimal moisture content and stuffing for 24h. The test was loaded at 0, 50, 100, 200, 300, 400, 500, 600, 700 and 800 kpa. When the displacement within 1h of a certain load was less than 0.01 mm, the sample was considered stable, and then the next level was applied successively until all loads were loaded. The compression modulus and compression index of gravel soil were then obtained.

3.2 Test steps

Xu *et al.* (2020) carried out a model test in a road test tank surrounded by rigid constraints. This limited the diffusion of the tamping energy so that the measured value of compactness in the model test was larger than that in the actual project under the same conditions. Based on previous studies, we analyzed the layered settlement of subgrade under different drop distance and tamping times. The effective reinforcement depth was obtained by combining peak rammer acceleration at the moment of tamping and the layered compactness before and after reinforcement. Considering different material properties, the dimensionless

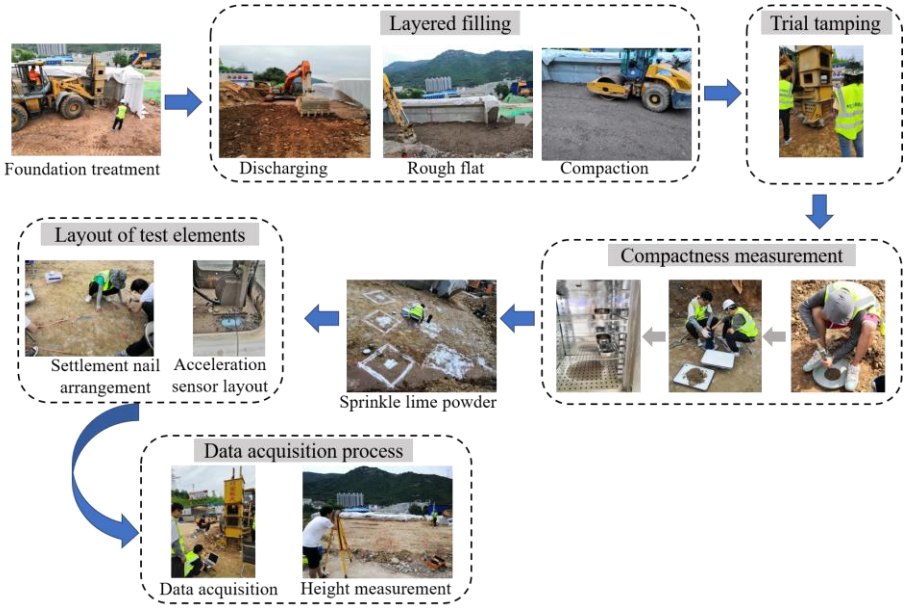

Fig. 5 Flow chart of field test

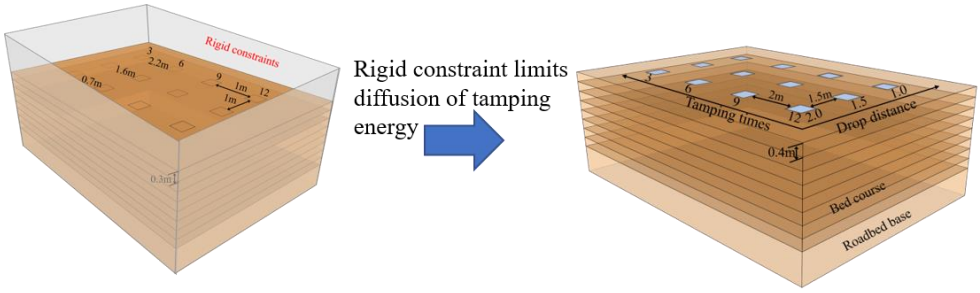

Fig. 6 Layout of tamping points

equation of the layered compactness within the effective reinforcement depth was established.

An HHT-66 hydraulic compactor was used for the field test, which had a rammer weight of 3t and a bottom side length of 0.7 m. The field layout scheme is shown in Fig. 5. The tamping energy range of the hydraulic compactor is 0~6 6kJ, the drop distance of the rammer is 0~2.2 m, the tamping frequency could reach 30 times/min, and the system pressure was 20~25 MPa.

Tamping point spacing (*s*) is an important parameter in reinforcement, which is consistent with the conclusion in the literature (Carter *et al.* 2015, Allouzi *et al.* 2019, Mollamahmutoglu and Avci 2018). When the tamping point spacing is small, the mutual extrusion of soil caused by the interaction between tamping points makes the effective reinforcement range larger than the actual reinforcement range (Yang *et al.* 2004). Therefore, as there is little research on the lateral influence range of hydraulic compaction, the tamping point spacing is determined using dynamic compaction. Finally, the lateral influence range is obtained as (He 2006, Hu 2007)

$$\left.\begin{aligned} H &= \varphi\sqrt{0.1Qh} \\ L &= r+\sqrt{2}\nu H \end{aligned}\right\} \Rightarrow L = r+\sqrt{2}\nu\varphi\sqrt{0.1Qh} \tag{22}$$

Where R is the side length of the rammer; φ is the correction coefficient, which is taken as 0.5 in this paper; ν is Poisson's ratio, which is taken as 0.32.

We conservatively calculated the lateral influence range based on the maximum drop distance (h_{max}=2.0 m), obtaining a lateral influence range of L_{max}=1.26 m. The rammer compresses the surrounding soil laterally during the ramming process, resulting in negative displacement of early settlement. Yang *et al.* proposed that the tamping point spacing is generally determined according to the nature of soil and the required reinforcement depth. In order to facilitate the dissipation of excess pore water pressure, the tamping point spacing should not be too small, so as not to form a dense layer in the shallow layer during tamping and affect the transmission of tamping energy to the deep. On the other hand, the ramming pit produced by the previous ramming reduces the lateral restraint, whereby subsequent re-ramming can easily cause ramming pit collapse and rammer skew, which will affect the reinforcement effect. Considering the economy of dynamic compaction project, the on-site tamping point spacing was set to 2.0 m/1.5 m (s> L_{max}), which is more than twice the diameter of rammer.

As the construction parameters are related to the subgrade filler, we selected three non-influencing points for

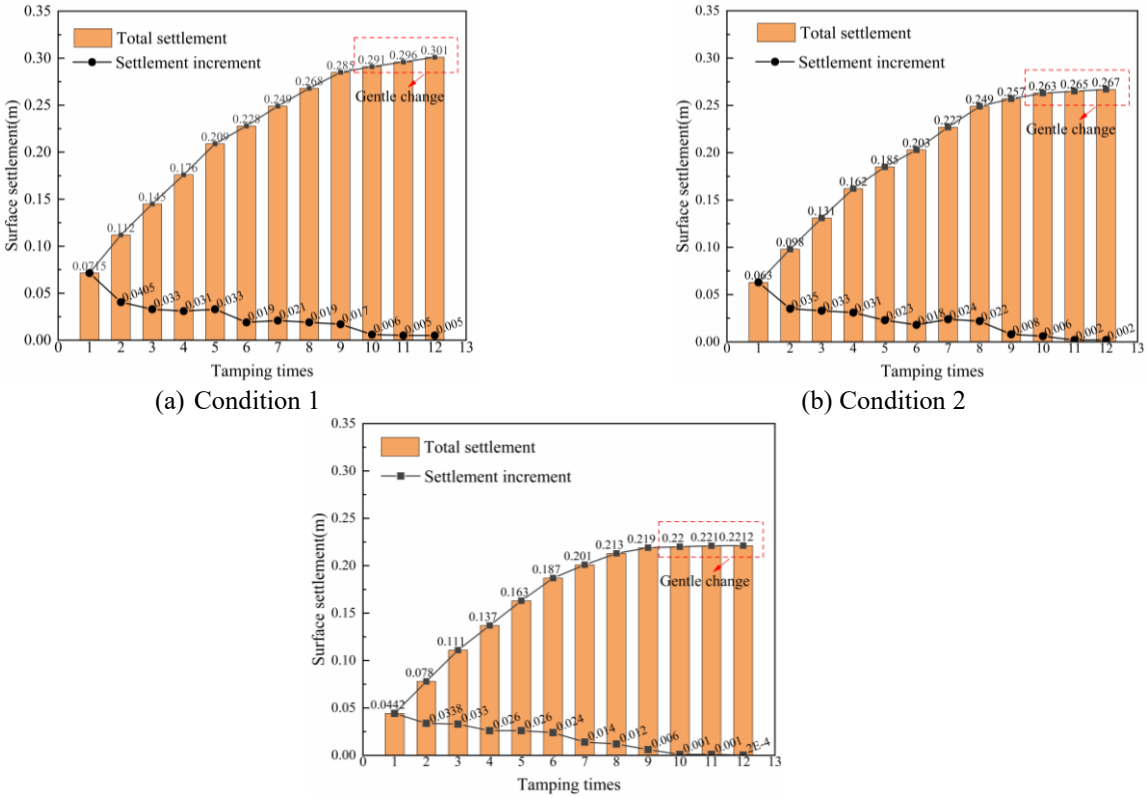

(a) Condition 1 (b) Condition 2

(c) Condition 3

Fig. 7 Schematic diagram of surface settlement of subgrade under different drop distances

trial tamping to determine the maximum tamping times. According to the trial tamping results, the maximum tamping times is determined as 12. As shown in Fig. 5, layered paving is carried out at 0.4m during construction, and the roller compaction difference is less than 0.2 cm, which is considered to meet the requirements (JTG/T 3610-2019). In the process of subgrade filling, each layered interface was marked using white powder. Settlement nails were buried at each layered interface in the center of the tamping point (Fig. 6), and the initial elevation was recorded using a leveling instrument. When the reinforcement was completed, the tamping points were excavated layer by layer from the surface of the subgrade. The elevation change of the settlement nail was then measured to determine the settlement of each layer interface after reinforcement. A DH5902N data acquisition instrument was connected with an acceleration sensor, the acquisition parameters were set, and data acquisition was performed.

4. Test results and discussion

4.1 Soil displacement analysis

4.1.1 Settlement analysis of soil surface at the center of tamping point

The curves of the settlement with tamping times under three conditions are obtained and combined with the settlement results of the hydraulic compactor to better study the deformation characteristics of the subgrade. It can be seen from Fig. 7 that the variation trend of total settlement under the three conditions is the same and shows a positive correlation with the drop distance of the rammer. At the same time, the settlement increment of the subgrade decreases with increasing tamping times. The settlement curve can be divided into the accelerated descent stage *i*, the deceleration descent stage *ii*, and structural failure stage *iii*.

In the accelerated descent stage *i* (1~6 blows), the loose pores or overhead structures in the soil are damaged under compaction, resulting in significant settlement of the subgrade and speed of settlement is rapid. The deceleration stage *ii* (7~9 blows) belongs to the re-compaction stage of soil, which is dominated by small changes in the pores between particles. The decrease in settlement speed indicates that the soil at this stage gradually adapts to the new dynamic system, tends to stabilize, and achieves compactness. The soil settlement in the structural failure stage *iii* (10~12 blows) approaches zero. The soil at this stage will hardly be compressed, and plastic deformation will occur instead, which will cause the soil around the tamping pit to bulge upwards. The above phenomenon is consistent with the principle of soil tamping and strengthening.

4.1.2 Layered settlement analysis at the center of tamping point

The curves of tamping times and layered settlement under three conditions are shown in Fig. 8. It can be seen that there is a positive correlation between tamping times and settlement,

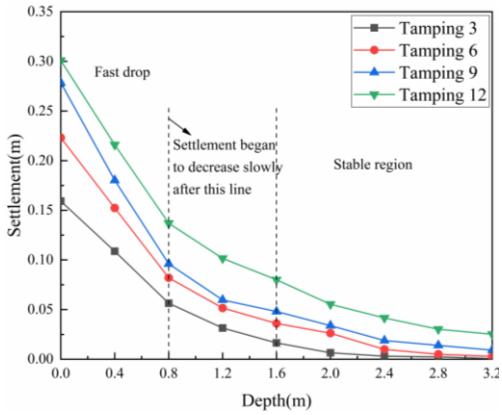

(a) Condition 1

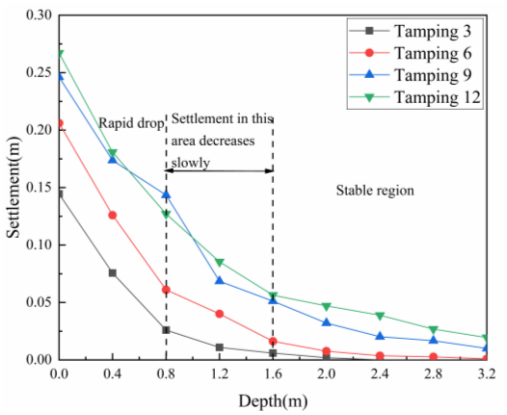

(b) Condition 2

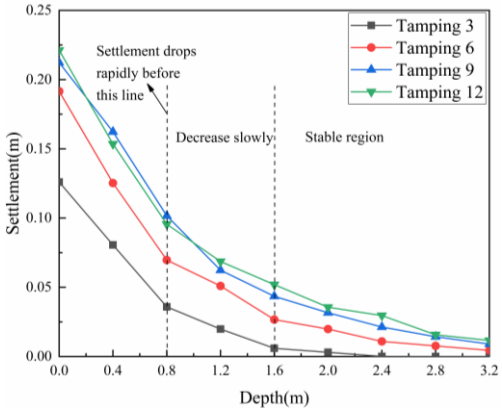

(c) Condition 3

Fig. 8 Curve of layered settlement under different conditions

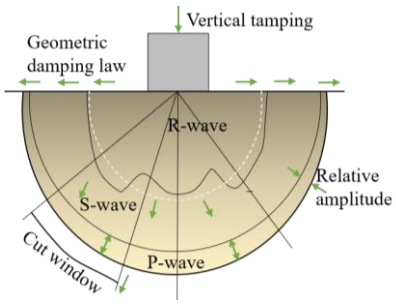

(a) Wave field generated by foundation during compaction

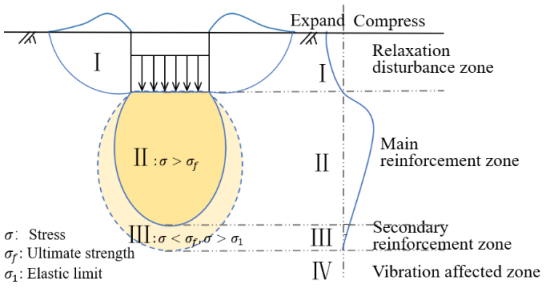

(b) Schematic diagram of reinforcement

Fig. 9 Schematic diagram of rammer foundation interaction

and the settlement growth rate gradually slows down and eventually stabilizes. When the depth of the subgrade is 0~0.8 m, the settlement decreases with increasing depth and decelerates rapidly. When the depth is 0.8~1.6 m, the deceleration of settlement decreases. And when the depth exceeds 1.6 m, the settlement is small and gradually tends to be gentle. This is because different forms of shock waves are generated when the rammer tamps the soil, which are transmitted into the subgrade to compact the soil. The wave speed decreases with the increase of depth, as shown in Fig. 9(a). This is consistent with our interpretation of dynamic load (Nazhat and Airey 2015). Moreover, according to the stress distribution relationship of the subgrade, it can be divided into relaxation disturbance, main reinforcement, secondary reinforcement and vibration affected zone (Fig. 9(b)). Therefore, the determine the effective reinforcement depth must be determined to fully understanding the reinforcing effect and prevent waste ramming.

4.2 Peak acceleration analysis of rammer

The curve of peak acceleration is shown in Fig. 10. The peak acceleration of conditions 1, 2 and 3 at 12 blows are 2126, 1852 and 926 m/s^2, respectively. The results show that the peak acceleration increases with the increase of drop distance. The peak acceleration of the rammer also gradually rises with increasing tamping times, but its increase rate gradually stabilizes. This is mainly because, for the soil that

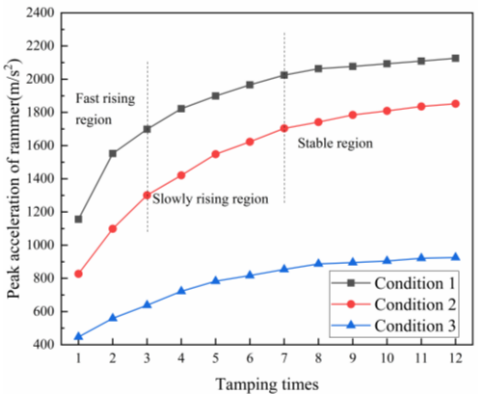

Fig. 10 Schematic diagram of peak acceleration of rammer under different conditions

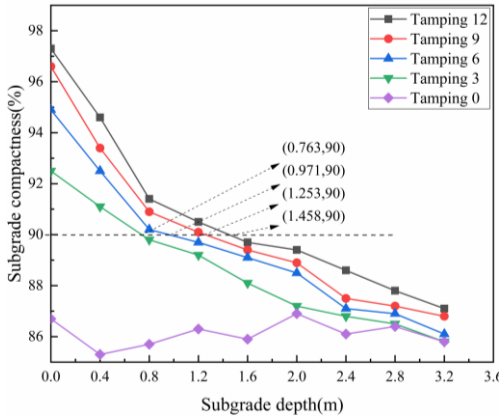

(a) Condition 1

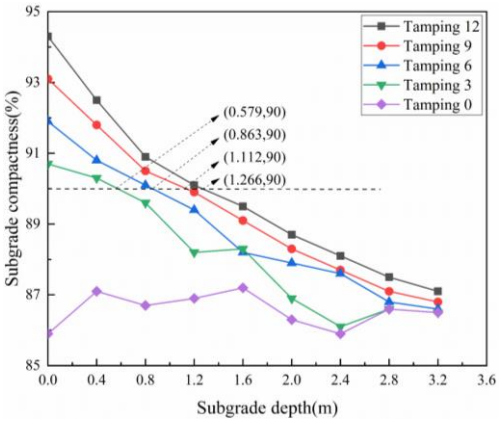

(b) Condition 2

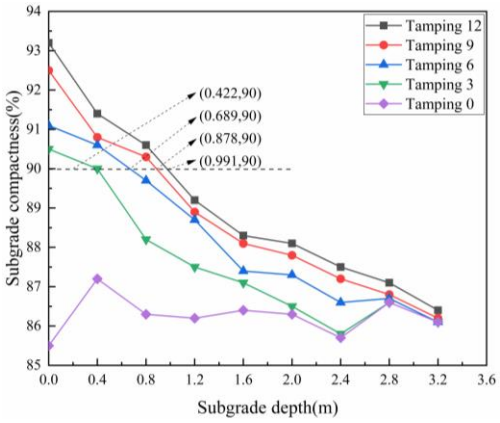

(c) Condition 3

Fig. 11 Schematic diagram of layered compactness under different conditions

has not yet been tamped, the depth of soil along the subgrade gradually becomes harder as tamping times increase. The different compactness of subgrade makes the absorption degree of tamping energy different. The denser the subgrade, the less ramming energy absorbed by the soil, the more energy is reflected back, and the greater the tamping response signal detected by the acceleration sensor on the rammer. This finding is similar to the previous conclusions on dynamic response (Tian *et al.* 2018). The earlier analysis shows that tamping is a process in which the soil is gradually compacted with the increase of tamping times, but the rate gradually slows down, which explains why the increasing rate of peak acceleration decreases gradually.

4.3 Determination of effective reinforcement depth

Combined with Fig. 11, the effective reinforcement depth of different tamping times under three conditions are obtained, as shown in Table 3. There are many factors affecting the effective reinforcement depth, mainly including the nature of soil, the bottom area of rammer, the drop distance of rammer, the tamping times and the tamping energy of rammer (weight × drop distance), which affects the effective reinforcement depth directly. The difference of the effective reinforcement depth in this table is mainly caused by the drop distance of rammer and tamping times.

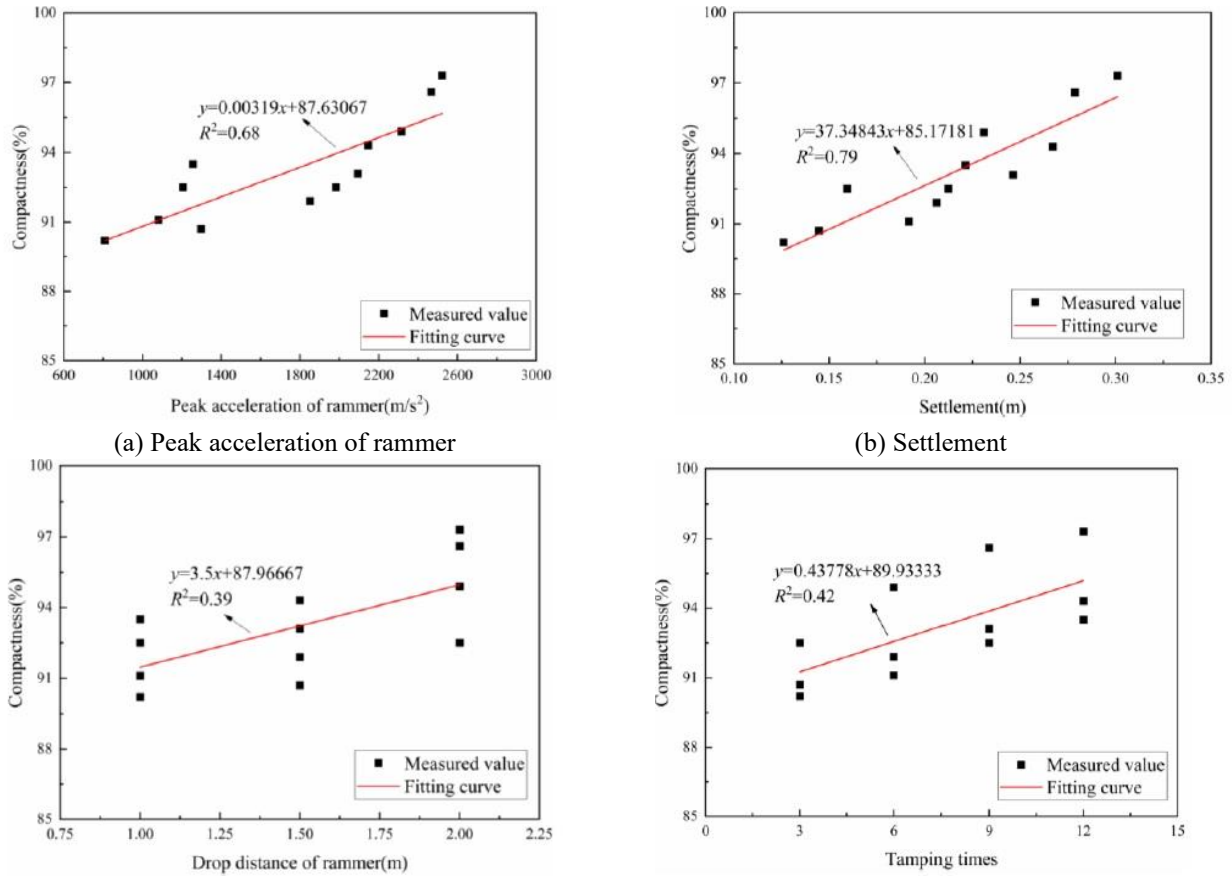

(a) Peak acceleration of rammer (b) Settlement

(c) Drop distance of rammer (d) Tamping times

Fig. 12 Linear fitting relationship between compactness and key parameters

Table 3 The effective reinforcement depth under the tamping times

Tamping times	Drop distances		
	Condition 1 (2.0 m)	Condition 2 (1.5 m)	Condition 3 (1.0 m)
3	0.763	0.579	0.422
6	0.971	0.863	0.689
9	1.253	1.112	0.878
12	1.458	1.266	0.991

Similar to the variation law of peak acceleration, Fig. 11 shows that the effective reinforcement depth increases with the increasing tamping times. The greater the tamping energy, the greater the effective reinforcement depth at the same tamping times, but the growth rate gradually tends to be flat. This is because with the increasing tamping times, the soil becomes more and more dense, and the impact on the soil becomes smaller and smaller. When a certain number of tamping times is reached, the additional stress generated by impact loading in the soil is close to yield stress within the affected depth. The stress state is within the yield surface and is not enough to significantly change the soil yield surface's spatial position, size and shape. At this time, the increase rate of the effective reinforcement depth will approach 0.

4.4 Derivation of dimensionless model

4.4.1 Prediction model of surface compactness

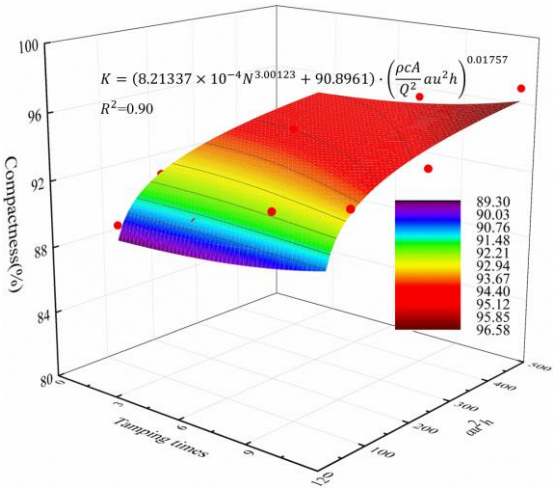

Fig. 13 Fitting of surface compactness

Figs. 12(a)-12(d) show the scattering results when the subgrade compactness is expressed as a single parameter function of u, a, h and N, respectively. The following conclusions can be drawn from the results in Figs. 12(a)-12(d). First, the correlation between compactness and single parameter is poor, while plotting au^2h, N as a function of compactness for nonlinear surface fitting leads to a satisfactory correlation. The values of u, a, h, N and K are shown in Figs. 7, 8, 10 and 11, and the other parameters used for model fitting are shown in Table 4.

Table 4 Value of argument

Density /kg·m^{-3}	Cohesion /Pa	Rammer			
		Weight /kg	Bottom area /m^2	Tamping times	Drop distance /m
2058	25230	30000	0.7×0.7	3/6/9/12	2.0/1.5/1.0

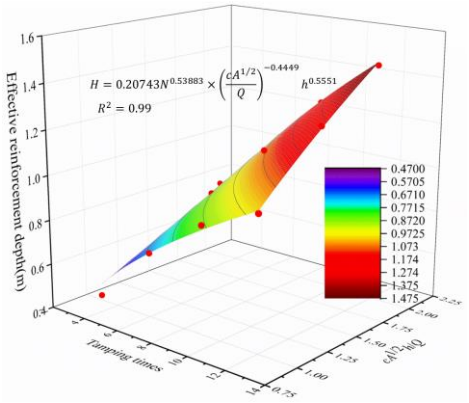

Fig. 14 Fitting of effective reinforcement depth

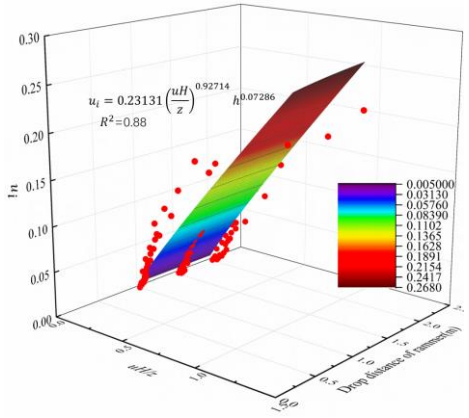

Fig. 15 Fitting of layered settlement

As shown in Fig. 13, the compactness obtained from field test is fitted, and the correlation is 0.90. A confidence interval at 95% is estimated, and the maximum deviation between the measured and calculated value is only 1.24%. Thus, for 95% of the predictions, the relative error between the calculated and measured values is less than 1.24%, confirming that the prediction of compactness by dimensional analysis is effective. Finally, the calculation equation for the compactness of the subgrade surface is obtained as

$$K=\left(8.21337\times10^{-4}N^{3.00123}+90.8961\right)\cdot\left(au^2h\cdot\rho cA/Q^2\right)^{0.01757} \quad (23)$$

4.4.2 Prediction model of effective reinforcement depth

A schematic diagram of the effective reinforcement depth fitting for gravel soil subgrade reinforcement is shown in Fig. 14. The dimensional analysis shows that there is a functional relationship between N, $cA^{1/2}h/Q$ and the effective reinforcement depth. According to nonlinear surface fitting, the calculation equation of effective reinforcement depth is obtained, and the fitting correlation is 0.99.

$$H=0.20743\cdot N^{0.53883}\left(cA^{1/2}/Q\right)^{-0.4449}h^{0.5551} \quad (24)$$

4.4.3 Prediction model of layered settlement

The settlement of deep soil is difficult to determine when the subgrade is reinforced. According to the previous analysis, it can be known that there is a functional relationship between uH/z, h and the layered settlement. Therefore, u, h, Z and H are used to represent the displacement of deep soil. Fig. 15 shows the fitting of the layer settlement, where the layered settlement is obtained (fitting correlation 0.88).

$$u_i=0.23131\cdot(uH/z)^{0.92714}h^{0.07286} \quad (25)$$

Fig. 15 also shows the fitting of the settlement within a depth of 3.2 m, and that the effective reinforcement depth measured on-site is 0.422 m~1.458 m. The fitted curve shows that the larger errors are mainly concentrated outside the effective reinforcement depth. Therefore, it can be concluded that the prediction model of layered settlement based on dimensional analysis is reliable.

4.4.4 Prediction model of layered compactness

Similarly, there is a power function relationship between K_i and au_i^2h, N within the effective reinforcement depth. Fig. 16 shows the nonlinear surface fitting, where the R^2 is 0.91. Therefore, the layered compactness can be expressed as

$$K_i=\left(144.89058N^{-0.0056}-52.10025\right)\cdot\left(au_i^{\,2}h\cdot\rho cA/Q^2\right)^{0.01159} \quad (26)$$

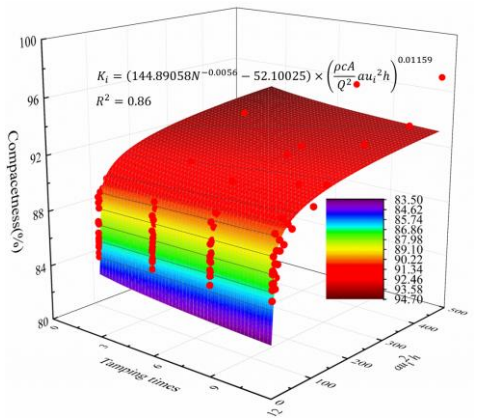

Fig. 16 Fitting of layered compactness

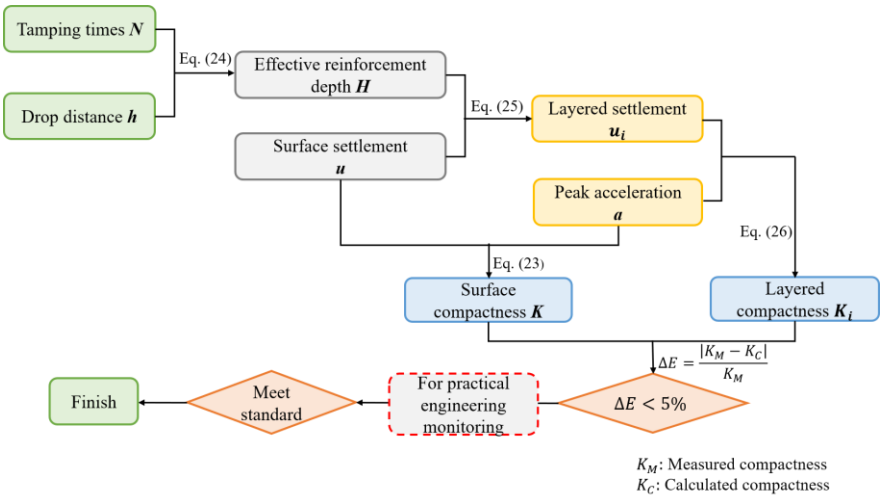

Fig. 17 Guide diagram of compaction quality calculation based on hydraulic compaction method

Table 5 Parameters of references

Density /kg·m^{-3}	Cohesion /Pa	Rammer			
		Weight /kg	Bottom area /m^2	Tamping times	Drop distance /m
1610	15470	30000	0.7×0.7	3/6/9/12	2.2/1.6/0.7

Table 6 Calculated values of K and H

h /m	N	a /m·s^{-2}	u /m	K /%	H /m
2.2	3	1462	0.24	92.34	0.91
	6	1737	0.31	93.65	1.33
	9	1846	0.35	94.58	1.65
	12	1979	0.36	95.68	1.93
1.6	3	1000	0.23	91.07	0.77
	6	1174	0.27	92.06	1.11
	9	1426	0.30	93.10	1.38
	12	1630	0.32	94.41	1.62
0.7	3	815	0.13	87.80	0.48
	6	1033	0.17	89.12	0.70
	9	1145	0.19	90.02	0.88
	12	1210	0.20	91.04	1.02

Combined with the field test and theoretical analysis, the subgrade settlement and peak acceleration of the rammer can reflect the compaction quality. Therefore, based on the previous analysis, the surface settlement of the subgrade and peak acceleration of the rammer can be used to calculate the compactness. A guide diagram illustrating the analysis process is shown in Fig. 17.

5. Application case analysis

5.1 validation for prediction model

This section aims to verify the efficiency of the prediction model proposed in this paper. The test data from Xu *et al.* (2010) was used for validation, and the model parameters used in the validation were listed in Table 5, where the packing density is calculated according to the maximum dry density and initial compactness. In the study by Xu *et al.* (2020), the tamping times were 3, 6, 9 and 12 blows, and the drop distances of the rammer were 2.2, 1.6, and 0.7 m, respectively. The entire model test was carried out in a test tank, with a length of 108 m, a width of 10 m and depth of 2.5 m.

This paper establishes a series of prediction model for the surface compactness, the effective reinforcement depth, the layered settlement and the layered compactness based on dimensional analysis and field test data. In this section, the proposed prediction model is used to incorporate the model test parameters (c、ρ、A、Q、N), and is compared with the measured values by Xu *et al.* to verify reliability. The

Table 7 Calculated values of u_i and K_i

h /m	z /m	N											
		3			6			9			12		
		u_i /m	K_i /%		u_i /m	K_i /%		u_i /m	K_i /%		u_i /m	K_i /%	
			K_C	K_M		K_C	K_M		K_C	K_M		K_C	K_M
2.2	0	0.24	92.34	92.27	0.31	93.65	94.96	0.35	94.58	97.19	0.36	95.68	98.10
	0.3	0.18	90.58	90.90	0.33	91.46	92.87	0.45	91.86	94.90	0.53	92.08	96.08
	0.6	0.1	89.24	90.72	0.17	90.10	92.16	0.23	90.50	93.93	0.28	90.72	95.24
	0.9	0.07	88.46	89.48	0.12	89.32	90.01	0.16	89.71	90.67	0.19	89.94	91.65
	1.2	-	-	-	0.09	88.77	87.99	0.12	89.16	88.97	0.15	89.38	89.50
	1.5	-	-	-	-	-	-	0.1	88.73	87.47	0.12	88.95	87.93
1.6	0	0.23	91.07	91.16	0.27	92.06	92.72	0.30	93.10	93.70	0.32	94.41	94.54
	0.3	0.14	89.37	89.79	0.24	90.06	90.83	0.32	90.54	91.67	0.39	90.90	92.52
	0.6	0.08	88.05	89.33	0.13	88.72	90.10	0.17	89.2	90.75	0.21	89.55	91.47
	0.9	-	-	-	0.09	87.95	88.60	0.12	88.43	89.18	0.14	88.78	89.77
	1.2	-	-	-	-	-	-	0.09	87.88	88.14	0.11	88.23	88.52
	1.5	-	-	-	-	-	-	-	-	-	0.09	87.81	87.41
0.7	0	0.13	87.80	90.14	0.17	89.12	91.18	0.19	90.02	91.77	0.20	91.04	92.36
	0.3	0.05	86.31	89.43	0.1	87.13	90.02	0.13	87.58	90.54	0.16	87.82	90.93
	0.6	-	-	-	0.05	85.84	89.83	0.07	86.29	90.16	0.08	86.52	90.81
	0.9	-	-	-	-	-	-	-	-	-	0.06	85.77	89.71

*Note: "-" indicates no value

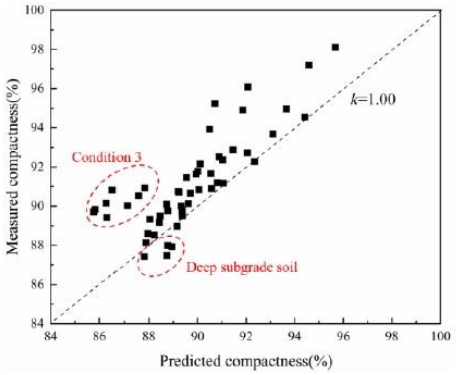

(a) Comparison of prediction ability of layered compactness, the line corresponds to 1:1 relationship

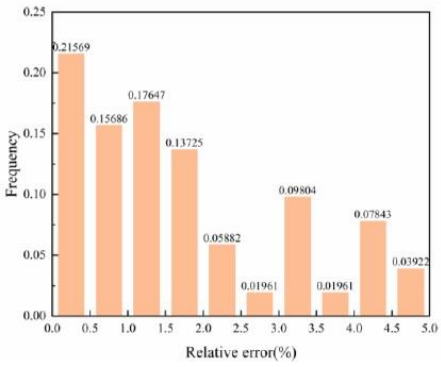

(b) Error probability distribution histogram

Fig. 18 Predictive model

calculated values of surface compactness and the effective reinforcement depth using the proposed prediction model are shown in Table 6. Moreover, the calculated layered settlement and layered compactness within the effective reinforcement depth are shown in Table 7.

The predicted and measured layered compactness are compared in Fig. 18(a) in order to assess the accuracy. For each tamping point, the difference between the measured value and the prediction is plotted as an error histogram in Fig. 18(b). The scattered points in Fig. (18) are near the straight line with a slope of 1 (k=1), which shows that the subgrade compactness from the proposed prediction and measured model are overall close, despite a little of difference. Moreover, the predicted value of compactness is lower than measured. This is due to the rigid constraints around the test tank, which limit the diffusion of tamping energy to a certain extent, thereby improving the compactness. As a result, the actual measured compactness by Xu *et al.* (2020) is slightly larger than the subgrade site under the same conditions.

The histogram of error frequency distribution calculated by compactness is shown in Fig. 18(b), illustrating that 76% of the calculation shave an error less than 3%. The probability of error between 2.5% and 5.5% is about 25%, which is mainly concentrated in the deep of soil and condition 3. The compactness of the deep soil has little effect on the stability of the subgrade. On the other hand, the tamping point under condition 3 is close to the boundary of the test tank, so that the soil reinforcement was based on rigid constraints analysis,

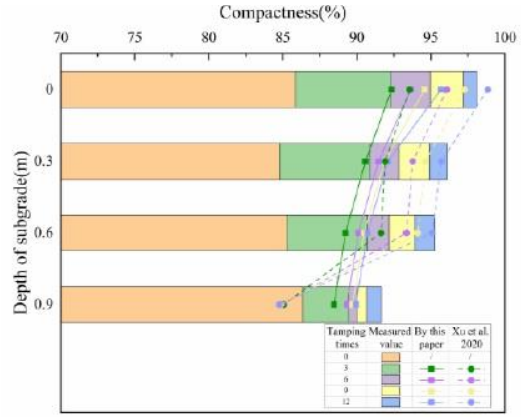

Fig. 19 Comparison of layered compactness prediction models

which affect the values of compactness evaluation. Given the limitations of the model test, the calculated results are considered to be in acceptable agreement with the measured compactness.

5.2 Comparison for prediction model

The prediction model proposed in this paper and proposed by Xu *et al.* (2020) are compared to perform an overall validation, as shown in Fig. 19. In the study by Xu *et al.* (2020), the peak acceleration of the rammer (a), the effective reinforcement depth (H), the settlement (u) and compactness (K) under the different drop distance (h) and tamping times (N) were obtained through the model test, and proposed a layered compactness monitoring method for reinforcing subgrade with a hydraulic compactor. The calculation process is the layered compactness (K_i) and the peak acceleration of rammer (a) within the effective reinforcement depth could be well fitted by a quadratic function model (K_i=A$_i a^2$+$B_i a$ +C_i), in which the parameters A_i, B_i and C_i are the fitting coefficients for each layered.

However, Xu *et al.* (2020) ignored influence of dimensional unification, the construction parameters and the subgrade filler, making the calculated layered compactness are quite different and slightly larger than the measured data at depth (z)=0.6 to 0.9 within the effective reinforcement depth. Meanwhile, the layered compactness by the prediction model proposed in this paper was more analogous with measured data. The prediction of compactness is particularly important for construction quality. If the calculated compactness is slightly smaller than actual compactness, an adequate amount of surplus space will be left, which will improve the safety of the subgrade and pavement engineering. Furthermore, our prediction model appears to reflect the trend of layered compactness using a hydraulic compactor. While there are some differences in the deep soil, this soil has little influence on the stability, and some errors are caused by the field measurement collection process. Therefore, the calculated layered compactness is considered to be in good agreement with the measured results. To summarize, the results using the prediction model are similar to the experiment in both qualitative and numerical terms. Thus, the model is reasonable and can be used to predict the layered compactness of the subgrade.

6. Conclusions

This study examined the compactness of deep soil based on dimensional analysis. In-situ reinforcement tests of gravel soil subgrade in the Taibai-Fengxian Expressway in Shaanxi Province were carries out using a hydraulic compactor. According to the changes of subgrade parameters before and after reinforcement, the prediction model of compactness within the effective reinforcement depth was obtained. The main conclusions can be summarized as follows:

- The functional relationship between the peak acceleration of the rammer, the settlement, and subgrade compactness was established based on the analysis of the factors influencing the reinforcement effect. A compactness prediction model by dimensional analysis was then proposed.
- The results show that there were differences in the reinforcement effect inside the subgrade. The increase rate of compactness and the settlement decrease with increasing subgrade depth. The compactness and settlement increased faster at a depth of 0~0.8m. The increase rate then gradually slow down and finally stabilized.
- The compactness could be described by the settlement of the subgrade and the peak acceleration of the rammer within the effective reinforcement depth using dimensional analysis. A power function relationship was demonstrated among the combined physical quantities of the rammer, the compactness and the subgrade filler.
- Compared with predecessors, our prediction model considers the influencing factors of reinforcement and dimension. The calculated compactness in this paper is slightly lower than the measured compactness, which is safer for subgrade monitoring. The prediction model has been verified by engineering, and the error is within the allowable range. Thus, the model is considered to have universal applicability.

Acknowledgments

The research described in this paper was financially supported by the National Key R & D Program of China (No. 2018YFC0808706) and the Project on Social Development of Shaanxi Provincial Science (No. 2018SF382).

References

Adam, D., Adam, C. and Falkner F.J. (2011), "Vibration emission induced by Rapid Impact Compaction", *Proceedings of the 8th international conference on structural dynamics*, 914-921, Leuven, Belgium, August.

Allouzi, R., Bodour, W.A.L. Alkloub, A. and Tarawneh, B. (2019), "Finite-element model to simulate ground-improvement technique of rapid impact compaction", *Proceedings of the institution of civil engineers-ground improvement*, **172**(1), 44-52. https://doi.org/10.1680/jgrim.18.00057.

Anderegg, R. and Kaufmann, K. (2004), "Intelligent compaction with vibratory rollers-Feedback control systems in automatic

compaction and compaction control", *Transport. Res. Rec*., **1868**, 124-134. https://doi.org/10.3141/1868-13.

Arias-Lara, D. and De-la-Colina, J. (2018), "Assessment of methodologies to estimate displacements from measured acceleration records", *Measurement*, **114**(2018), 261-273. https://doi.org/10.1016/j.measurement.2017.09.019.

Bai, T., Yang, H., Chen, X.B., Zhang, S.C. and Jin, Y.S. (2020), "In-situ monitoring and reliability analysis of an embankment slope with soil variability", *Geomech. Eng*., **23**(3), 261-273. https://doi.org/10.12989/gae.2020.23.3.261.

Barman, M., Nazari, M., Imran, S.A., Commuri, S. and Zaman, M. (2016), "Quality Improvement of Subgrade Through Intelligent Compaction", *Transport. Res. Rec*., **2579**(1), 59-69. https://doi.org/10.3141/2579-07.

Butterfield, R. (2001), "Dimensional analysis for geotechnical engineers", *Geotechnique*, **49**(3), 357-366. https://doi.org/10.1680/geot.51.1.91.39352.

Buzzi, O. (2010), "On the use of dimensional analysis to predict swelling strain", *Eng. Geol*., **116**(1-2), 149-156. https://doi.org/10.1016/j.enggeo.2010.08.005.

Buzzi, O., Giacomini, A. and Fityus, S. (2011), "Towards a dimensionless description of soil swelling behaviour", *Geotechnique*, **61**(3), 271-277. https://doi.org/10.1680/geot.7.00194.

Cai, H.B., Kuczek, T., Dunston, P.S. and Li, S. (2017), "Correlating intelligent compaction data to in situ soil compaction quality measurements", *J. Constr. Eng. M*., **143**(8), 04017038. https://doi.org/10.1061/(ASCE)CO.1943-7862.0001333.

Cai, J., Wang, Y.Y. and Luo, M.D. (2013), "Model tests on the layout of punning position in dynamic compaction for loess", *Appl. Mech. Mater*., **2685**(813), 304-309. https://doi.org/10.4028/www.scientific.net/AMM.405-408.304.

Carter, J.P., Sabetamal, H., Nazem, M. and Sloan S.W. (2015), "One-dimensional test problems for dynamic consolidation", *Acta Geotech*., **10**(1), 173-178. https://doi.org/10.1007/s11440-014-0336-x.

Dimitrakopoulos, E., Makris, N. and Kappos, A.J. (2009b), "Dimensional analysis of the earthquake-induced pounding between adjacent struc-tures", *Earthq. Eng. Struct. D*., **38**(7), 867-886. https://doi.org/10.1002/eqe.872.

Dimitrakopoulos, E., Makris, N. and Kappos, A.J. (2010), "Dimensional analysis of the earthquake response of a pounding oscillator", *J. Eng. Mech*., **136**(3), 299-310. https://doi.org/10.1061/(ASCE)0733-9399(2010)136:3(299).

Dobrzycki, P., Kongar-Syuryun, C. and Khairutdinov, A. (2019), "Vibration reduction techniques for Rapid Impulse Compaction (RIC)", *J. Phys.: Conference Series*, **1425**(1), 012202. http://doi.org/10.1088/1742-6596/1425/1/012202.

Erem yants, V.I. and Uraimov, M. (2009), "Dynamics of hydraulic vibration machine for soil compaction", *J. Mach. Manuf. Reliab*., **38**(5), 425-430. https://doi.org/10.3103/S1052618809050033.

Feng, S.J., Hu, B., Zhang, X. and Shui, W.H. (2012), "Model test study on impact parameters' influence on tamping effect", *J. Tongji U.* (Natural S.), **40**(8), 1147-1153. https://doi.org/10.3969/j.issn.0253-374x.2012.08.005.

Ghanbari, E. and Hamidi, A. (2014), "Numerical modeling of rapid impact compaction in loose sands", *Geomech. Eng*., **6**(5), 487-502. https://doi.org/10.12989/gae.2014.6.5.487.

Gruzin, A.V., Gruzin, V.V. and Shalay, V.V. (2018), "Model dynamics of a rammer's operating element in a soil foundation of a tank for liquid hydrocarbons storage", *AIP. Conf. Proc.*, **2007**(1), 030009. https://doi.org/10.1063/1.5051870.

He, C.M. (2006), "Experiment and Research on strengthening high embankment by dynamic compaction method", M.D. Dissertation, Central South University, Changsha.

Herrera, C., Costa P.A. and Caicedo, B. (2018), "Numerical modelling and inverse analysis of continuous compaction control", *Transp. Geotech*., **17**, 165-177. https://doi.org/10.1016/j.trgeo.2018.09.012.

Hu, C.M., Wang, Y.Y., Mei, Y., Yuan, Y.L. and Zhang, S.S. (2018), "Compaction techniques and construction parameters of loess as filling material", *Geomech. Eng*., **15**(6), 1143-1151. https://doi.org/18.15.6.1143.

Hu, N.C. (2007), "Study on design parameters of foundation reinforcement by dynamic compaction method", M.D. Dissertation, Shandong University, Jinan.

Hua, T.B., Yang, X.G., Yao, Q. and Li, H.T. (2018), "Assessment of real-time compaction quality test indexes for rockfill Material based on roller vibratory acceleration analysis", *Adv. Mater. Sci. Eng*., **2018**, 1-15. https://doi.org/10.1155/2018/2879321.

Huang, S.G., Wang, L.J. and Wang, K. (2014), "Application and Numerical Simulation of dynamic compaction on collapsible loess subgrade", *Proceeding of the 3rd International Conference on Railway Engineering*, Beijing, China, July.

JTG E40-2007 (2007), Test Methods of Soils for Highway Engineering[S]. Beijing: People's Communications Press.

JTG/T 3610-2019 (2019), Technical Specifications for Construction of Highway Subgrades, Ministry of transport of the people's Republic of China; Beijing, China.

Kodikara, J., Islam, T. and Sounthararajah, A. (2018), "Review of soil compaction: History and recent developments", *Transp. Geotech*., **17**, 24-34. https://doi.org/10.1016/j.trgeo.2018.09.006.

Li, C. (2018), "Study on Effective Reinforcement Depth of Dynamic Compaction of Backfilled Sand Foundation", M.D. Dissertation, China University of Geosciences, Beijing.

Ling, J.M., Lin, S., Qian, J.S., Zhang, J.K., Han, B.Y. and Liu, M. (2018), "Continuous compaction control technology for granite residual subgrade compaction", *J. Mater. Civil Eng*., **30**(12), 255-261. https://doi.org/10.1061/(ASCE)MT.1943-5533.0002522.

Ma, Z.Y., Dang, F.N. and Liao, H.J. (2014), "Numerical study of the dynamic compaction of gravel soil ground using the discrete element method", *Granular Matter*., **16**(6), 881-889. https://doi.org/10.1007/s10035-014-0529-x.

Mayne, P.W., Jones, J.S. and Dumas, J.C. (1984), "Ground response to dynamic compaction", *J. Geotech. Eng. ASCE*, **110**(6), 757-774. https://doi.org/ 10.1061/(ASCE)0733-9410(1984)110:6(757).

Meehan, C.L., Cacciola, D.V., Tehrani, F.S. and Baker, W.J. (2017), "Assessing soil compaction using continuous compaction control and location-specific in situ tests", *Automat. Constr*., **73**, 31-44. https://doi.org/10.1016/j.autcon.2016.08.017.

Meehan, C.L., Tehrani, F.S. and Vahedifard, F. (2012), "A comparison of density-based and modulus-based in situ test measurements for compaction control", *Geotech. Test. J*., **35**(3), 387-399.

Mei, Y., Hu, C.M., Yuan, Yuan, Y.L., Wang, X.Y. and Zhao, N. (2016), "Experimental study on deformation and strength property of compacted loess", *Geomech. Eng*., **11**(1), 161-175. https://doi.org/10.12989/gae.2016.11.1.161.

Min, Y.Z., Tao, J. and Ren, W.Z. (2020), "A high-precision online monitoring system for surface settlement imaging of railway subgrade", *Measurement*, **159**, 107707. https://doi.org/10.1016/j.measurement.2020.107707.

Mollamahmutoglu M. and Avci E. (2018), "Dynamic compaction experience in alluvial soils of Carsamba (Turkey)", *Maejo. Int. J. Sci. Tech*., **12**(03),206-220. https://doi.org/

Nazhat, Y. and Airey, D. (2015), "The kinematics of granular soils subjected to rapid impact loading", *Granul. Matter.*, **17**(1), 1-20. https://doi.org/10.1007/s10035-014-0544-y.

Nie, Z.H. (2011), "Comparison experimental study on subgrade compaction quality test methods", *Appl. Mech. Mater*., **71-78**,

4679–4684. https://doi.org/10.4028/www.scientific.net/AMM.71-78.4679.
Parvizi, M. (2009), "Soil response to surface impact loads during low energy dynamic compaction", *J. Appl. S*., **9**(11), 2088-2096. https://doi.org/10.3923/jas.2009.2088.2096.
Pistrol, J. and Adam, D. (2018), "Fundamentals of roller integrated compaction control for oscillatory rollers and comparison with conventional testing methods", Transp. Geotech., **17**, 75-84. https://doi.org/10.1016/j.trgeo.2018.09.010.
Rinehart, R.V., Mooney, M.A, Facas, N.F. and Musimbi, O.M. (2012), "Examination of roller-Integrated continuous compaction control on Colorado test site", *Transp. Res. Rec*., **2310**(1), 3-9. https://doi.org/10.3141/2310-01.
Sabbar, A.S., Chegenizadeh, A. and Nikraz, H. (2018), "Effect of slag and bentonite on shear strength parameters of sandy soil", *Geomech. Eng*., **15**(1), 659-668. https://doi.org/10.12989/gae.2018.15.1.659.
Senseney, C.T. and Mooney, M.A. (2010), "Characterization of two-layer soil system using a lightweight deflectometer with radial sensors", *Transp. Res. Rec*., **2186**(1), 21-28. https://doi.org/10.3141/2186-03.
Tehrani, F.S., Meehan, C.L. and Vahedifard, F. (2014), "Comparison of density-based and modulus-based in situ tests for earthwork quality control", *Geotech. Spec. Publ*., (234 GSP), 2345-2354. https://doi.org/10.1061/9780784413272.228.
Thilakasiri, H.S., Gunaratne, M., Mullins, G., Stinnette, P. and Jory, B. (1996), "Investigation of impact stresses induced in laboratory dynamic compaction of soft soils", *Int. J. Numer. Anal. Met*., **20**(10), 753-767. https://doi.org/10.1002/(SICI)1096-9853(199610)20:10<753:AID-NAG846>3.0.CO;2-R.
Tian, L.S. Chen, H.K., Sun, Y.L., Zhang, Q.H. and Liao, H.R. (2018), "Traffic-load-induced dynamic stress accumulation in subgrade and subsoil using small scale model tests", *Geomech. Eng*., **16**(2), 113-124. https://doi.org/10.12989/gae.2018.16.2.113.
Torrijo, F.J., Garzon-Roca, J., Alija, S. and Quinta-Ferreira, M. (2017), "Dynamic compaction evaluation using in situ tests in Sagunto's Harbor, Valencia (Spain)", *Environ. Earth Sci*., **76**(19), 658. https://doi.org/10.1007/s12665-017-7033-7.
Viyanant, C., Rathje, E.M. and Rauch, A.F. (2004), "Compaction control of crushed concrete and recycled asphalt pavement using nuclear gauge", *Proceeding of Geotechnical Engineering for Transportation Projects v.1(Geo-Trans 2004)*, **126**, 958-966, Los Angeles, CA, USA, January.
Wang, X.B. (2011), "Experimental study on Application of on-line compactness detection technology", M.D. Dissertation, Chang'an University, Xi'an.
Wang, Y.X. and Liao, Y. (2012), "Experiment research of the lateral properties and density variation of loess subgrade to dynamic compaction for mountainous highway", *Appl. Mech. Mater*., **1975**(412), 1571-1574. https://doi.org/10.4028/www.scientific.net/AMM.204-208.1571.
Wersall, C., Nordfelt, I. and Larsson, S. (2018), "Resonant roller compaction of gravel in full-scale tests", *Transp. Geotech*., **14**, 93-97. https://doi.org/10.1016/j.trgeo.2017.11.004.
White, D.J., Jaselskis, E.J., Schaefer, V.R. and Cackler, E.T. (2005), "Real-Time Compaction Monitoring in Cohesive Soils from Machine Response", *Transp. Res. Rec*., **1936**, 173-180. https://doi.org/10.3141/1936-20.
Wu, Q.Y., Wang, T., Ge, H.B. and Zhu, H.P. (2019), "Dimensional analysis of pounding response of an oscillator based on modified Kelvin pounding model", *J. Aerosp. Eng*., **32**(4), 04019039. https://doi.org/10.1061/(ASCE)AS.1943-5525.0001018.
Wu, Y.K., Sang, X.S. and Niu, B. (2012), "High-speed hydraulic compactor application in the bacdkfilled of bridge platform", *Appl. Mech. Mater*., **212-213**, 1201-1204. dimensional10.4028/www.scientific.net/AMM.212-213.1201.
Xia, D.C. and Li, W.L. (2015), "Dynamic compaction real-time detection based on acceleration measurement", *J. Vib. Shock*, **34**(15), 45-50. https://doi.org/10.13465/j.cnki.jvs.2015.15.009.
Xing, H.F., Liu, L.L. and Luo, Y. (2019), "Water-induced changes in mechanical parameters of soil-rock mixture and their effect on talus slope stability", *Geomech. Eng*., **18**(4), 353-362.https://doi.org/10.12989/gae.2019.18.4.353.
Xing, X.M., Chen, L.F., Yuan, Z.H. and Shi, Z.N. (2019), "An improved time-series model considering rheological Parameters for surface deformation monitoring of soft clay subgrade", *Sensors*, **19**(14), 3073. https://doi.org/10.3390/s19143073.
Xu, J.B., Li, H., Du, K., Yan, C.G, Zhao, X., Li, W., and Xu, X.Z. (2018), "Field investigation of force and displacement within a strata slope using a real-time remote monitoring system", *Environ. Earth. Sci*., **77**(15). https://doi.org/10.1007/s12665-018-7729-3.
Xu, M., Song, E.X. and Cao, G.X. (2009), "Compressibility of broken rock-fine grain soil mixture", *Geomech. Eng*., **1**(2), 169-178. https://doi.org/10.12989/gae.2009.1.2.169.
Xu, T.Y., Zhou, Z.J., Yan, R.P., Zhang, Z.P., Zhu, L.X., Chen, C.R., Xu, F. and Liu, T. (2020), "Real-time monitoring method for layered compaction quality of loess subgrade based on hydraulic compactor reinforcement", *Sensors*, **20**(15), 4288. https://doi.org/10.3390/s20154288.
Xu, W.J., Li, C.Q. and Zhang, H.Y. (2015), "DEM analyses of the mechanical behavior of soil and soil-rock mixture via the 3D direct shear test", *Geomech. Eng*., **9**(6), 815-827. https://doi.org/10.12989/gae.2015.9.6.815.
Yan, B., Lin, P.Y. and Yu, H.T. (2011), "Analysus of settlement and tamping energy dissipation", *Chinese J. Geotechnic*, **33**(S1), 249-252.
Yang, J.G., Peng, W.X. and Liu, D.Y. (2004), "Research of choosing tamping factors for dynamic consolidation method", *Rock Soil Mech*., **2004**(8), 1335-1339. https://doi.org/10.16285/j.rsm.2004.08.035.
Yao, Y.P. and Zhang, B.Z. (2016), "Reinforcement range of dynamic compaction based on volumetric strain", *Rock Soil Mech*., **37**(9), 2663-2671. https://doi.org/10.16285/j.rsm.2016.09.031
Zhang, D.Z. and Xiong, Z.Q. (2008), "Calculation of dispersion curve by combined cross-spectrum and phase shift method and its application to evaluate compactness of subgrade", *Proceeding of the 3rd International Conference on Environmental and Engineering Geophysics*, Wuhan, China, June.
Zhang, G.X., Yuan, Z.X., Wang, N., Zhang, Z.Z. and Gao, P. (2013), "Dynamic Response Analysis of Compaction Loess Subgrade", *Adv. Mat. Res*., **671-674**, 202-208. https://doi.org/10.4028/www.scientific.net/AMR.671-674.202.
Zhang, Y., Liu, J.K., Fang, J.H. and Xu A.H. (2013), "Application of dynamic compaction and rolling compaction in the subgrade improvement of Qarhan-Golmud Highway", *Sci. Cold Arid Reg*., **5**(5), 603-607. https://doi.org/10.3724/SP.J.1226.2013.00603.
Zhang, Z.P., Zhou, Z.J., Guo, T., Xu, T.Y., Zhu, L.X., Xu, F., Chen, C.R., and Liu, T. (2021), "A measuring method for layered compactness of loess subgrade based on hydraulic compaction", *Meas. Sci. Technol*., **32**(5), 055106. https://doi.org/10.1088/1361-6501/abd7ab.
Zhou, S.Y., Kang, Y.L., Xie, H.M., Wang, L.H. and Zhang, Q. (2019), "An approach integrating dimensional analysis and field data for predicting the load on tunneling machine", *KSCE J. Civ. Eng*., **23**(7), 3180-3187. https://doi.org/10.1007/s12205-019-0266-0.

IC